Detecting Unauthorized Changes to Urban Boundaries using Photogrammetry Products

Muhammad Amin Bakhshi [1]*, Mehrdad Eslami [2], Ali Sarkargar Ardakani[3]

[1] PhD Student of Remote Sensing & GIS, Imam Hussain University, Tehran, Iran - m.a.bakhshi.rs@ihu.ac.ir
[2] Dept. of Geomatic Engineering, Imam Hussain University, Tehran, Iran - meslami@ihu.ac.ir
[3] Dept. of Geomatic Engineering, Imam Hussain University, Tehran, Iran - aliardakani@yahoo.com

KEY WORDS: Change Detection, DSM, Unauthorized Construction, Photogrammetry Products, Urban Management.

ABSTRACT:

Change detection has a history spanning over four decades in military and civilian applications. Monitoring and controlling urban changes, particularly identifying unauthorized land-use changes, is essential for urban management. Traditional methods lack efficiency due to limitations in accuracy, speed, and comprehensiveness, while newer deep learning approaches face challenges like training data preparation, time-consuming processes, and high computational demands. This paper proposes a relatively fast, low-cost, and high-accuracy method using photogrammetric products with planar and vertical accuracies better than 30 cm. By applying thresholds and filters, a Digital Difference Model (DDM) is generated to detect changes in residential areas. Overall accuracy in two test sites exceeded 90% and 83%, respectively. Disturbing features were removed by masking Orthophotomosaics using intelligent algorithms. Applying optimized filters in four stages improved accuracy by over 30%. While the process depends on regional characteristics and urban-specific thresholds, its lower cost and higher speed make it widely applicable to similar areas. For regions with different urban textures, optimal thresholds and parameters must be recalculated using the same methodology.

1. INTRODUCTION

1.1 General Instructions

Change detection in geomatics has extensive applications in military and civilian domains, including monitoring enemy fortifications, damage assessment, map updating (Hamidi & Bigdeli, 2021), urban management, environmental monitoring, crisis management, and detecting unauthorized constructions. This technology is also used in agriculture (monitoring plant growth), natural resource management (detecting illegal logging), archaeology, geology, and air traffic management (Moghimi et al., 2016). High-resolution time-series remote sensing data, particularly drone-based photogrammetric products, enable three-dimensional (length, width, height) change analysis, ideal for monitoring unauthorized constructions requiring height change assessment.

Change detection methods include pattern matching, object-based image analysis (OBIA), and deep learning (e.g., convolutional neural networks) (Cheng & Han, 2016). These methods, comparing dual-time data, achieve high accuracy (up to 97%) in building detection (Masoumi et al., 2021; Guerin et al., 2014). However, shadows and vegetation cause errors (Sanin et al., 2012). Advanced methods, such as DSMs and graph-cut algorithms (Pang et al., 2019) or multimodal networks (Xie et al., 2024, with an F1 score of 79.29%), improve accuracy by mitigating shadows and vegetation effects (Guo et al., 2024). The NDVI index also aids in shadow removal (Gao et al., 2018). A multimodal joint learning framework for building change detection, training a Siamese dual-time image network and a height difference (HDiff) network with labeled source data and unlabeled target data pairs, using vanilla, integrated, and separate joint learning, achieved an optimal F1 score of 79.29% (Xie et al., 2024). Additionally, the Multi-scale Feature Fusion Network (MFFNet), using 1-meter pixel DSMs from satellite imagery, accurately detected building changes in China by eliminating vegetation and shadow effects (Guo et al., 2024).

The proposed method integrates photogrammetric data and Orthophotomosaic classification to detect building height changes, eliminating interferences like shadows and vegetation. Using thresholding and time-series data, it offers high accuracy in monitoring unauthorized constructions.

2. LITERATURE REVIEW

2.1 2.1 Supervised Image Classification

To eliminate interfering features (e.g., shadows, vegetation) from orthophotomosaic images and detect buildings, the Maximum Likelihood classification method is employed. This method, per Equation (1), classifies pixels based on band count and similarity to training samples (Hamidi & Bigdeli, 2021).

$$PX(X)=Exp(-1/2\ln|\sum k|(1/2\sum_{k}^{-1}(X-mk) \quad (1)$$

Where n is the number of input bands,X is the pixel in n bands, and PX(X) is the probability of pixel X belonging to class k. Classification accuracy is evaluated using overall accuracy and the Kappa coefficient.

2.2 Validation and Accuracy Assessment of the Proposed Process

The proposed process, combining three components to generate various events, requires evaluating algorithm accuracy in detecting targets in remote sensing images to identify the most accurate event. A confusion matrix compares ground truth with algorithm predictions for each event, calculating overall accuracy based on the ground truth map, resulting in four possible scenarios (Hamidi & Bigdeli, 2021).

In summary, the performance of the proposed process is evaluated based on identified targets across four scenarios: True Positive (TP, ground truth positive and predicted positive), False Positive (FP, ground truth positive and predicted negative), False Negative (FN, ground truth negative and

* Corresponding author

predicted positive), and True Negative (TN, ground truth negative and predicted negative).

$$\text{Accuracy} = TP + TN / \ TP + TN + FP + FN \quad (2)$$

The accuracy evaluation metrics for target detection algorithms include:

2.1.1 Overall Accuracy

The accuracy of an algorithm is valid in TP and TN scenarios, where targets are correctly identified or correctly excluded as non-targets. According to Equation (2), this metric is calculated as the ratio of correctly identified elements to the total number of events across all scenarios. It assesses the algorithm's quality (Hamidi and Bigdeli, 2021).

2.1.2 Kappa Coefficient

Using the confusion matrix, the Kappa coefficient compares the algorithm's performance to a random classifier, indicating how much better it performs. It is calculated per Equation (3). The coefficient ranges from -1 to +1, where values closer to +1 indicate higher agreement between scales, and values closer to -1 indicate lower agreement. A Kappa of zero signifies complete disagreement.

$$\text{Kappa} = Pr(a) – Pr(e) / \ 1- Pr(e) \quad (3)$$

3. IDENTIFICATION OF THE PROPOSED PROCESS COMPONENTS

The proposed process is executed using three components: height threshold, area threshold, and length-to-width ratio, with the method for determining optimal values for each component described as follows:

3.1 Height Threshold

To determine the optimal height threshold for the building class in urban areas, as shown in Figure 1, the Digital Difference Model (DDM) is analyzed across various height ranges. By applying different height thresholds, feature behavior is examined in ranges of 0–1 m, 1–5 m, and 1 m to the maximum DDM value. Residential buildings are not discernible below 1 m, but above 1 m, they exhibit consistent behavior, forming a continuous surface indicative of a building. Limiting the threshold to a specific range reduces the likelihood of including the feature in final targets due to discontinuous segments.

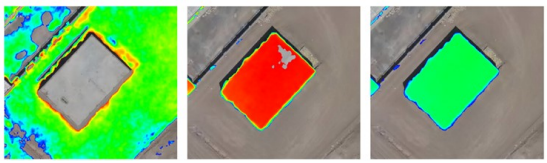

Figure 1. Analysis of height changes at different thresholds using the Digital Difference Model (DDM). a) Validation of the DDM in the 0–1 m range. b) 1–5 m range. c) 1 m to the maximum DDM value.

3.2 Area Threshold

After extracting pixels exceeding the height threshold, the area of the identified target at a uniform height is connected to form a continuous surface. An area threshold is then applied to distinguish it from other features. The optimal area threshold is determined through trial-and-error and validation. In the first study area (Yazd), with a DDM pixel size of 40 cm (0.16 m² per pixel), the area representing a complete building is identified, and detection accuracy is assessed. In the second study area (Mehriz), with a 10 cm pixel size (0.01 m² per pixel), standardization between the two areas is required. The threshold, validated by examining 10 buildings absent in the first image but present in the second (indicating construction), isolates features by.

3.3 Length-to-Width Ratio

In urban and non-urban areas, features like vehicles, with heights ranging from 0.5 m (passenger cars) to 3.5 m (buses, trailers), are present. To eliminate vehicles from final results, the length-to-width ratio (major-to-minor axis) of features identified in prior steps is calculated, filtering out those exceeding a specific threshold. This component also identifies walls, edges, and boundaries that meet height and area thresholds but are not buildings and must be excluded. As shown in Figure 2, passenger cars have a length-to-width ratio similar to building components (e.g., parapets) but are removed earlier due to their smaller area. The proposed process combines these components, generating various events with different values, and selects optimal values based on accuracy validation (Hamidi & Bigdeli, 2021).

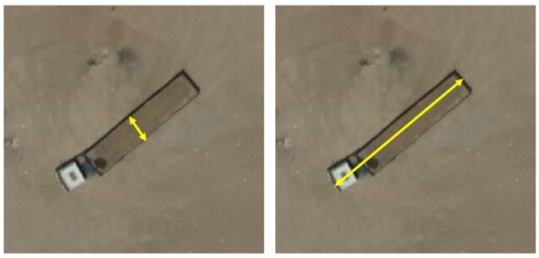

Figure 2. Analysis of changes in geometric components of features. a) Minor axis (width). b) Major axis (length).

4. MATERIALS AND METHODS

The proposed method detects 3D changes in buildings and earthworks using high-resolution, multi-temporal photogrammetric data. A two-stage process generates a Digital Difference Model (DDM) from DSMs and applies thresholds to isolate changes, removing interfering features via post-classification comparison (Hamidi & Bigdeli, 2021). A shadow- and vegetation-free model improves target detection in residential areas. Ground truth maps and orthophotomosaics validate targets, with optimal parameters determined through accuracy metrics. Non-targets (e.g., vegetation, vehicles) are filtered using length-to-width ratios.

4.1 Study Area

The study covers urban areas in Yazd (1,200 m elevation) and Mehriz (1,400 m), using aerial photogrammetric data with a two-month interval for Yazd (March–April 2020) and three years for Mehriz (February 2019–April 2022).

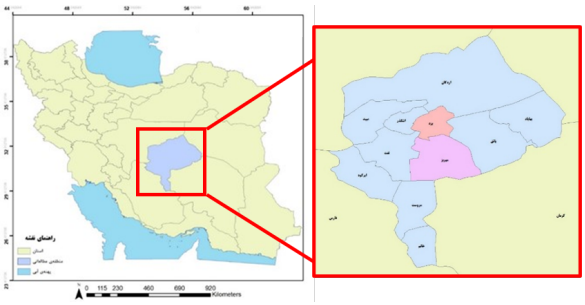

Figure 3. Map of the first study area (Yazd) and the second study area (Mehriz) and their geographical locations

4.2 Data Used

The specifications of the aerial photography equipment for both regions are presented in Table 2. The data preparation method involved aerial triangulation combined with ground control point processing, generating a dense point cloud through calculations of tie and key points, followed by the creation of a Digital Surface Model (DSM) and, finally, an Orthophotomosaic.

Row	1		2	
Study Area	First (Yazd)		Second (Mehriz)	
Time	1	2	1	2
Platform	Gyroplane	Crewed aircraft	DJI Phantom 4	Crewed aircraft
Camera	Phase One	FujiFilm GFX100	DJI Phantom 4	FujiFilm GFX100
GSD	6 cm	4 cm	2 cm	4 cm
F	100 mm	50 mm	8.8 mm	50 mm

Table 1. Data preparation tool specifications

Analysis in the first study area (Yazd) reveals height changes in buildings, building components (parapets, canopies), new roads, vehicle movements, earthworks, construction equipment, containers, kiosks, and vegetation. Orthophotomosaics for the first and second time periods have ground accuracies of 6 cm and 4 cm, respectively, with 10 cm pixel size. The Digital Surface Model (DSM) has a 30 cm height accuracy and 40 cm pixel size. The minimum and maximum heights in the first period are 1259.35 m and 1279.43 m, respectively, and in the second period, 1258.72 m and 1279 m.

Figure 4. Targets examined in the article: Buildings, building components (parapets and canopies), walls, earthworks, and vehicles.

Analysis in the second study area (Mehriz) reveals height changes in buildings, building components (parapets, canopies), new roads, vehicle movements, earthworks, pools, walls, land leveling, barren land cover, and vegetation. Orthophotomosaics for the first and second time periods have ground accuracies of 2 cm and 4 cm, respectively, with 10 cm pixel size. The Digital Surface Model (DSM) has a 30 cm height accuracy and 10 cm pixel size. Minimum and maximum heights in the first period are 1441.31 m and 1483.8 m, respectively, and in the second period, 1441.12 m and 1487.75 m.

The article's workflow, the initial step involves verifying the spatial co-registration of data from the first and second time periods. This ensures that the pixel positions of fixed features, such as a tower, a wall, or a building corner, which have not undergone geometric or height changes over time, are identical in both Orthophotomosaics and Digital Surface Models (DSMs). Due to the differing aerial photography times, this verification does not include shadow consistency.

Once spatial co-registration of data is confirmed, the Digital Difference Model (DDM) is generated by subtracting the first time period's Digital Surface Model (DSM) from the second, with pixel sizes matching the DSMs. The DDM displays height changes (e.g., a building's height increasing from 6 m to 9 m shows a 3 m change) and is insensitive to topography but affected by errors in photogrammetric processes like aerial triangulation or ground control points (Wu et al., 2016).

$$DDM = DSM_{T2} - DSM_{T1} \quad (4)$$

A Median filter smooths sharp points, and Orthophotomosaic classification (using Maximum Likelihood per Equation 1) removes shadows and vegetation, classified as noise, by setting their DDM pixels to zero (Wu et al., 2016). This enhances accuracy, but longer time intervals (>3 months) increase errors due to factors like sun angle changes (Shahtahmassebi et al., 2013). Classification may exclude valid targets if a shadow in the first image overlaps a new feature in the second.

Thresholding, determined via trial-and-error, involves height and area thresholds (Shahtahmassebi et al., 2013). Height thresholding creates a binary image, removing features below the threshold. Area thresholding groups adjacent pixels into continuous surfaces. For each target, five components are calculated: ID, X/Y coordinates, major/minor axes, and length-to-width ratio. Non-target features (e.g., buses, canopies) with high length-to-width ratios are filtered out using ground truth data.

	1	2	3	4	5
1	1	4.6246	160	196	2.5227
2	2	2.1637	155	132	2.6842
3	3	3.4572	158	138	1.3333
4	4	3.5155	156	183	3.7922
5	5	3.6832	159	168	2.3091
6	6	4.5345	99	170	3.3469
7	7	3.2603	168	148	1.5147
8	8	7.3066	114	170	2.0467
9	9	6.5124	157	166	1.7444
10	10	4.4825	104	192	2.2222
11	11	3.4808	174	149	1.4839
12	12	4.9171	128	149	1.2981

Figure 5. Calculated DN values for final targets - Columns 1 to 5 correspond to: target identifier, average Digital Difference Model (DDM) value across the target area, target center value in the T1 image, target center value in the T2 image, and the length-to-width ratio of the target.

Final targets meeting all criteria are displayed as a binary image and on the second time period's Orthophotomosaic, with target identifiers. Some targets may not align with ground truth. The proposed process's overall accuracy is calculated by comparing identified targets with ground truth using standard metrics.

Factors affecting detection accuracy are analyzed, and suggestions to minimize interfering factors are provided.
To identify targets (buildings and earthworks), ground truth maps for both study areas are created. Using the Digital Difference Model (DDM), pixels above a 1-meter height threshold are filtered and validated against Orthophotomosaics. Targets are manually identified and delineated. In Yazd, 41 targets, and in Mehriz, 65 targets were identified.

5. RESULTS AND DISCUSSION

It should be noted that the proposed process can only achieve similar results in areas similar to the study areas of this article. For example, in areas such as Tehran, where buildings are taller than the buildings in these areas, it is necessary to first test and evaluate different threshold values and then proceed to identify new buildings.

5.1 Identification of changes in built-up features (positive height changes)

5.1.1 First study area (Yazd city)

The results of implementing the proposed process, which was based on the three mentioned components, were carried out step by step in 20 different events. By counting the total number of targets identified by each event, the number of correct targets, the number of incorrect targets, and the number of embedded targets, the overall accuracy of identifying each event was calculated based on the accuracy evaluation criteria based on the confusion matrix. By sorting the results, based on the overall accuracy component from lowest to highest value, the highest overall accuracy is obtained in the event with a height threshold of 1 meter, an area threshold of 200 pixels, and a length to width ratio of 3.5, which is 0.905 (90.5%). Also, the kappa coefficient in this case reaches 0.921. Therefore, the values of the components of this event are examined in the second study area (Mehriz city) and their results are compared with each other.

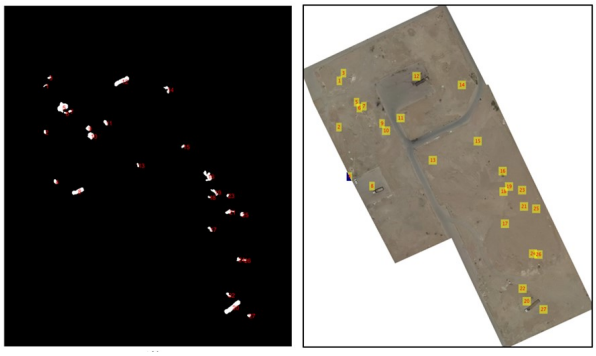

Figure 6. Output of the proposed process. (Left) In the binary output image, the final targets are shown in white, and their corresponding counters are displayed in red above each target. (Right) The corresponding display of the final targets over the Orthophotomosaic of the second epoch.

5.1.2 Second study area (Mehriz city)

The pixel size of the digital difference model of this area is 10 centimeters (0.01 square meters). According to the parameters determined in the first study area (Yazd city), the value of 200 pixels for the area threshold, which is equal to 32 square meters, is converted to 3200 pixels, equal to 32 square meters, by applying a coefficient of 16 to equate this value in the second study area (Mehriz city). By applying this coefficient, 150 pixels are converted to 2400 pixels. The results of implementing the proposed process in the second study area (Mehriz city) show that applying a height threshold of 1 meter and an area threshold of 200 pixels achieves the best results; however, by changing the length to width ratio from 3.5 to 4, more reliable results are obtained. In such a way that in the event with a length to width ratio of 4, with a one-unit decrease in the number of error targets, the overall accuracy in the highest case increases by about 3 percent, from 80.8 percent to 83.6 percent. The kappa coefficient is also obtained to be 0.934.

5.2 Analysis and evaluation of the effect of applying filters on the results of the proposed process

To evaluate the results of applying noise removal filters to the digital difference model, it is necessary to calculate the effect of applying or not applying them on the final results. Therefore, considering the results of the first study area (Yazd city) and the event with the highest overall accuracy (90.5%), at this stage, only this case was examined. Initially, all filters and the length-to-width ratio component were excluded from the implementation process. In this way, increasing the number of calculated targets (TP) and reducing the number of embedded targets (FN) are positive results of not applying the said filters. In such a way that all ground reality targets are identified and there will be no unidentified targets. However, we are faced with a multiple increase in the number of false targets (FP). As a result, the accuracy evaluation criteria also show a significant decrease. So that the overall accuracy decreases by 22% to 0.683.
In the next step, the proposed process was implemented with all filters except the classification filter. By doing this, the number of calculated targets increases and the number of embedded targets decreases. So that all targets are identified in accordance with the ground reality and there are no embedded targets. On the other hand, we are faced with a multiple increase in the number of false targets. As a result, the accuracy evaluation criteria also show a significant decrease. So that the overall accuracy reaches 0.759.
By not applying the edge removal filter, the number of calculated targets and the number of embedded targets are the same as the original event. But the number of false targets increases. As a result, the overall accuracy reaches 0.884. Finally, by not applying the length to width ratio, the number of calculated targets is equal to the original event; However, the number of embedded targets decreases and the number of false targets increases. As a result, the overall accuracy reaches 0.826. The results of the evaluation with and without filters are shown in Table 2.

Criteria	No. Target	TP	FP	FN	OA	K
Main	39	38	1	3	0.905	0.921
Without Filters	60	41	19	0	0.683	1.0
Without Classification	54	41	13	0	0.759	1.0
Without Edge	40	38	2	3	0.884	0.921
Without Geometry	44	38	6	2	0.826	0.923

Table 2. Comparison of the results of applying and not applying filters to the algorithm in the selected results of the first study area (Yazd city)

5.3 Discussion and review of results

The most important factors in the differences in the results of implementing the proposed process in the two study areas are the different conditions of the two areas in terms of the pixel dimensions of the input data and the time interval and season of their two times of photography, relative to each other. Because with the same implementation components for the two areas in the same events, different results are obtained; However, the implementation process and the final result are acceptable for the application of identifying and detecting new constructions.

By examining the results of not applying different filters, it can be concluded that if the classification results that are applied to the implementation model of the proposed process to remove the effect of shadows and vegetation are not applied, all the ground reality targets are identified and no features are missed. However, the error in counting false targets increases sharply, which directly affects the overall accuracy and precision of the identified results and reaches the lowest value.

On the other hand, by not applying the edge smoothing filter and the aspect ratio component, the number of identified targets is equal to the original event; but in both cases, the error increases, which results in a decrease in the accuracy of the identified targets, which can be seen on the overall accuracy. Finally, in the absence of the edge filter, the number of unidentified targets is the same as the original event; but in the absence of the aspect ratio, we also see a decrease in the number of unidentified targets.

Among the filters applied to the digital difference model, the application and non-application of the edge filter does not have a significant effect on the final results and can be completely discarded; But according to Table 2 and compared to the original event, by reducing the number of false targets by one, the overall accuracy in the first study area (Yazd city) is the highest. Finally, by comparing the results of the proposed process with other studies conducted in the field of building change detection and extraction, it is observed that in recent years, the use of image and elevation data fusion approach to reduce detection errors and increase the accuracy of extracted targets is increasing. However, the most important limiting factor in building detection is the presence of shadows and vegetation, which show similar elevation behavior to buildings. To solve this problem, various researches have been conducted using various methods, datasets, and networks. For example, Guo and his colleagues, using the MFFNet network and using several different datasets, have been able to achieve an overall accuracy of 98% in detecting and extracting new buildings (Guo et al., 2024). In another study, Xie and his colleagues achieved an accuracy of nearly 80% in detecting and extracting buildings by combining deep learning methods and merging elevation data with images, as well as using labeled training methods. In neural networks, the main factor determining the performance of the network includes the preparation of training data, the training and evaluation process of the network, and the structure of the network itself. These factors play a key role in the execution speed and overall accuracy of the algorithms. In this paper, due to the implementation approach of the proposed process and the lack of the need to design and prepare the neural network, the process of extracting the desired targets is carried out at a higher speed than other related research.

More precisely, the implementation of the main process, including the preparation of the ground reality map, classification of Orthophotomosaic images, and generation of the digital difference model (DDM), which was carried out in different software environments, achieved results with an accuracy of more than 90% in less than an hour. It should be noted that achieving this level of accuracy depends on the geographical, topographic, and texture characteristics of the area in question.

6. CONCLUSION

Identifying and detecting changes in features is inevitable in urban management in order to increase the speed of dealing with various natural and unnatural phenomena. In this paper, a new process for identifying and detecting changes that have occurred over time was carried out, based on the integration of photogrammetric products, including digital surface models and Orthophotomosaics, based on the use of the height and spectral nature of the data. In this paper, using high spatial resolution data (10 and 40 cm) for two study areas, with the help of thresholding and filtering in several stages to the digital difference model that is obtained by subtracting two digital surface models of two periods, building changes were extracted with the aim of investigating and identifying unauthorized constructions, with an average accuracy higher than 86%. According to the results based on the discussions and analyses obtained, compared to deep learning methods based on neural networks, the relatively higher execution speed, the lack of the need for appropriate training data, and the easier preparation of the model are the strengths of this process. On the other hand, obstacles such as shadows and vegetation in the area disrupt the counting and identification of targets and are considered as errors, and eliminating their effect in a simple solution using the results of supervised classification and applying it to the digital difference model increases the final accuracy by up to 30%. In various military and civilian applications, the process proposed in this article can be used to identify and detect new positions, changes that have occurred in operational areas, and monitor and control the legal boundaries and privacy of military, urban, and non-urban areas; with the difference that the sensitivity to the type of changes will determine the implementation components of the proposed process in the desired area.

REFERENCES

Adeline, K.R., Chen, M., Briottet, X., Pang, S.K., Paparoditis, N., 2013: Shadow detection in very high spatial resolution aerial images: A comparative study. Isprs Journal of Photogrammetry and Remote Sensing, 80, 21-38. DOI: 10.1016/j.isprsjprs.2013.02.003

Cheng, G., Huang, Y., Li, X., Lyu, S., Xu, Z., Zhao, H., Zhao, Q., Xiang, S., 2024: "Change Detection Methods for Remote Sensing in the Last Decade: A Comprehensive Review" Remote Sensing 16, no. 13: 2355. DOI: 10.48550/arXiv.2305.05813

C. Guerin, R. Binet, M. Pierrot-Deseilligny, "Automatic Detection of Elevation Changes by Differential DSM Analysis: Application to Urban Areas," in IEEE Journal of Selected Topics in Applied Earth Observations and Remote Sensing, vol. 7, no. 10, pp. 4020-4037, Oct. 2014, doi: 10.1109/JSTARS.2014.2300509

Erdogan, M. and Yilmaz, A., 2018: 'Detection of building damage caused by Van Earthquake using image and Digital Surface Model (DSM) difference', International Journal of Remote Sensing, 40(10), pp. 3772–3786. doi: 10.1080/01431161.2018.1552816.

Gao, X., Wang, M., Yang, Y., Li, C., 2018: Building Extraction from RGB VHR Images using Shifted Shadow Algorithm. IEEE

Access. PP. 1-1. 10.1109. DOI: 10.1109/ACCESS.2018.2819705.

Goyal, V., Singh, R., Dhawley, M., Kumar, A., Sharma, S., 2023: Aerial Object Detection Using Deep Learning: A Review. In: Shukla, A., Murthy, B.K., Hasteer, N., Van Belle, JP. (eds) Computational Intelligence. Lecture Notes in Electrical Engineering, vol 968. Springer, Singapore. DOI: 10.1007/978-981-19-7346-8_8

Guo, Z., Pan, J., Xie, P., Zhu, L., Qi, C., Wang, X., Yang, Y., Wang, Y., Zhang, H., Ren, Z., 2024: "MFFNet: A Building Change Detection Method Based on Fusion of Spectral and Geometric Information." Geocarto International 39 (1). DOI: 10.1080/10106049.2024.2322053.

Han, W., Chen, J., Wang, L., Feng, R., Li, F., Wu, L., Tian, T., Yan, J., 2021: Methods for Small, Weak Object Detection in Optical High-Resolution Remote Sensing Images: A survey of advances and challenges. IEEE Geoscience and Remote Sensing Magazine. DOI: 10.1109/MGRS.2020.3041450

hamidi, M. A., bigdeli, H., 2021: 'damage assessment in military operations using deep learning and image processing', Journal of Soft Computing and Information Technology, 10(3), pp. 1-10.

Hong, F., Jianqing, Z., Zuxun, Z. et al. House change detection based on DSM of aerial image in urban area. Geo-spat. Inf. Sci. 2, 68–72, 1999: https://doi.org/10.1007/BF02826721

Ioannidis, C., Psaltis, C., Potsiou, C., 2009: Towards a strategy for control of suburban informal buildings through automatic change detection. Comput. Environ. Urban Syst., 33, 64-74. DOI: 10.1016/j.compenvurbsys.2008.09.010

Krauß, T., Tian, J., 2020: Automatic Change Detection from High-Resolution Satellite Imagery. In: Hadjimitsis, D., et al. Remote Sensing for Archaeology and Cultural Landscapes. Springer Remote Sensing/Photogrammetry. Springer, Cham. https://doi.org/10.1007/978-3-030-10979-0_4

Liang, H., Seo, S., 2023: "UAV Low-Altitude Remote Sensing Inspection System Using a Small Target Detection Network for Helmet Wear Detection" Remote Sensing 15, no. 1: 196. https://doi.org/10.3390/rs15010196

Masumei, A., Feizizadeh, B., Valizadeh Kamran, K., 2022: 'A novel semi-automated approach for detecting and extracting of urban features using object-based aerial image analysis', Journal of Geography and Planning, 26(80), pp. 315-303. doi: 10.22034/gp.2020.41630.2696

Moghimi A, Ebadi H, Sadeghi V. Review of Change Detection Methods from Multitempolar Satellite Images by Pixel-Based and Object-Based Approach. GEJ 2016; 7 (2) :99-110URL: doi: http://gej.issgeac.ir/article-1-170-en.html

Movia, A., Beinat, A., Crosilla, F., 2016: Shadow detection and removal in RGB VHR images for land use unsupervised classification. ISPRS Journal of Photogrammetry and Remote Sensing. 119. 10.1016/ DOI: 10.1016/j.isprsjprs.2016.05.004

Pang, S., Hu, X., Zhang, M., Cai, Z., Liu, F., 2019: Co-Segmentation and Superpixel-Based Graph Cuts for Building Change Detection from Bi-Temporal Digital Surface Models and Aerial Images. Remote Sensing, 11(6), 729. https://doi.org/10.3390/rs11060729

Raja, P., Kumar, S., Yadav, D.S., Kumar, A., Kumar, R.K., 2023: Intelligent Remote Sensing: Applications and Techniques. Journal of Image Processing and Intelligent Remote Sensing, 3(02), 46–53. https://doi.org/10.55529/jipirs.32.46.53

Zhu, Q., Guo, X., Deng, W., Shi, S., Guan, Q., Zhong, Y., Zhang, L., Li, D., 2022: Land-Use/Land-Cover change detection based on a Siamese global learning framework for high spatial resolution remote sensing imagery, ISPRS Journal of Photogrammetry and Remote Sensing, Volume 184, Pages 63-78, ISSN 0924-2716, https://doi.org/10.1016/j.isprsjprs.2021.12.005.

Sanin, A., Sanderson, C., Lovell, B., 2012: Shadow Detection: A Survey and Comparative Evaluation of Recent Methods. Pattern Recognition. 45. 1684-1695. DOI: 10.1016/j.patcog.2011.10.001

Shahtahmassebi, A.R., Yang, N., Wang, K., Moore, N.J., Shen, Z., 2013: Review of shadow detection and de-shadowing methods in remote sensing. Chinese Geographical Science, 23, 403-420. DOI: 10.1007/s11769-013-0613-x

Shi, W., Zhang, M., Zhang, R., Chen, S., Zhan, Z., 2020: "Change Detection Based on Artificial Intelligence: State-of-the-Art and Challenges" Remote Sensing 12, no. 10: 1688. https://doi.org/10.3390/rs12101688

Stilla, U., Xu, Y., 2023: Change detection of urban objects using 3D point clouds: A review, ISPRS Journal of Photogrammetry and Remote Sensing, Volume 197, Pages 228-255, ISSN 0924-2716, https://doi.org/10.1016/j.isprsjprs.2023.01.010.

Wu, C., Zhang, L., & Zhang, L., 2016: A scene change detection framework for multi-temporal very high resolution remote sensing images. Signal Process., 124, 184-197. DOI: 10.1016/j.sigpro.2015.09.020

Y. Xie, X. Yuan, X. X. Zhu and J. Tian, "Multimodal Co-Learning for Building Change Detection: A Domain Adaptation Framework Using VHR Images and Digital Surface Models," in IEEE Transactions on Geoscience and Remote Sensing, vol. 62, pp. 1-20, 2024, Art no. 5402520, doi: 10.1109/TGRS.2024.3362680.

Zhang, Yu et al., 2023: 'Mixed-former: multi-fusion remote sensing change detection', International Journal of Remote Sensing, 44(11), pp. 3507–3528. doi: 10.1080/01431161.2023.2224100.

Zhifang, L., Jianqing, Z., Zuxun, Z. et al. Change detection based on DSM and image features in urban areas. Geo-spat. Inf. Sci. 6, 35–41 (2003: https://doi.org/10.1007/BF02826752